ARTICLE

A Nanoengineering Approach for Investigation and Regulation of Protein Immobilization

Yih Horng Tan, Maozi Liu, Birte Nolting, Joan G. Go, Jacquelyn Gervay-Hague, and Gang-yu Liu*

Department of Chemistry, University of California, Davis, California 95616

ABSTRACT It is known that protein attachment to surfaces depends sensitively upon the local structure and environment of the binding sites at the nanometer scale. Using nanografting and reversal nanografting, both atomic force microscopy (AFM)-based lithography techniques, protein binding sites with well-defined local environments are designed and engineered with nanometer precision. Three proteins, goat antibiotin immunoglobulin G (IgG), lysozyme, and rabbit immunoglobulin G, are immobilized onto these engineered surfaces. Strong dependence on the dimension and spatial distribution of protein binding sites are revealed in antibody recognition, covalent attachment *via* primary amine residues and surface-bound aldehyde groups. This investigation indicates that AFM-based nanolithography enables the production of protein nanostructures, and more importantly, protein−surface interactions at a molecular level can be regulated by changing the binding domains and their local environment at nanometer scale.

KEYWORDS: nanografting · reversal nanografting · arrays of nanostructures · atomic force microscopy · self-assembled monolayers · polyvalent interactions · multipoint protein binding · protein immobilization · local structures

Much effort has been devoted recently to protein immobilization on surfaces because surface-bound proteins have important applications in drug screening, biosensing, bioassaying, and protein characterization.[1] Fundamental interactions between proteins and solid surfaces include one or a combination of physical adsorption,[2−7] electrostatic forces,[8] specific recognition,[9−11] and covalent binding.[3,6,12−14] These interactions are found to depend sensitively upon the local structures and environment of protein binding sites on surfaces.[15,16] Much work has been devoted to surface modification for protein adhesion, which has been reviewed and discussed extensively.[15,17−19] For example, the coverage and overall morphology of physically adsorbed bovine serum albumin (BSA) on mixed self-assembled monolayers (SAMs) depend upon the surface structure of the monolayer (*e.g.*, phase segregation or lateral heterogeneity).[20] Using a bilayer platform, Yang *et al.* reported that a higher binding affinity was observed for anti-dinitrophenyl-keyhole limpet hemocyanin IgG antibodies to high density hapten-containing membranes[13,21] in comparison to the monovalent binding of anti-dinitrophenyl-keyhole limpet hemocyanin IgG antibodies to hapten ligand. The apparent dissociation constant, K_{Dapp}, for the bivalent binding of an antibody to the hapten ligand decreased by about a factor of 10 as the ligand density increased.[13,21] Similar dependence of surface heterogeneity at the nanometer level was also demonstrated by Ostuni *et al.*[4] In their study, they found that the coverage of the adsorbed proteins *via* the interaction of the protein's hydrophobic groups with hydrophobic functional terminated molecules in a mixed SAM system increases as a function of the trityl terminal group's physical size ($-CH_2Ph < -CHPh_2 < -CPh_3$).[4] Theoretical approaches, such as the Temkin model and stoichiometric displacements model, have also been reported to deal with proteins' strong binding affinity due to multiple interactions between functional groups of the protein and the corresponding binding sites on surfaces.[22−24]

Prior approaches to regulating surface heterogeneity to affect protein immobilization mainly relied on a mixing-and-growth method due to its simplicity.[22] By regulating the composition of protein binding components and surface reaction conditions, this method was proven to be effective in changing surface domain structures and therefore impacted protein adhesion.[2,25] To attain a higher degree of control of protein−surface interactions, instead of relying on the tradeoff of thermal dynamics and kinetics of surface reactions in the mixing-and-growth, AFM-based nanolithog-

*Address correspondence to liu@chem.ucdavis.edu.

Received for review August 8, 2008 and accepted October 06, 2008.

Published online October 29, 2008. 10.1021/nn800508f CCC: $40.75

raphy techniques, such as nanografting,[25−27] were used in this investigation. AFM lithography is best known for the production of nanostructures of ligands, DNA, and proteins on surfaces.[4,28−30] To further take advantage of nanolithography, this work focuses on producing designed nanodomains of protein binding sites, with the precision of a single protein molecular size or smaller, and then characterizing protein molecules upon their interactions with these engineered surfaces *in situ*. The regulation of protein attachment to these engineered surfaces is clearly demonstrated.

RESULTS AND DISCUSSION

Nanografting and Reversal Nanografting. The concept and procedure of nanografting has been extensively discussed in our previous publications.[26,27,31] The key steps of nanografting, that is, imaging, shaving-and-replacement, and imaging again, are schematically shown in Figure 1. The matrix SAM is formed *via* natural growth, while thiol containing protein binding termini (or designed mixture) is in solution phase and is attached to the Au surface following the shaving trajectory of the AFM tip. For the investigation of protein adsorption, nanografting provides the simplest and very effective means for precise engineering of nanostructures with a designed single component[26] or with mixed components at controlled heterogeneity.[25] In the case of protein attachment *via* covalent binding between its primary amine groups and aldehyde termini on the substrate, a binary SAM of hexanethiol (referred to as C_6) and 11-mercapto-1-undecanal disulfide $[-S(CH_2)_{10}CHO]_2$ (referred to as $C_{10}CHO$ due to the cleavage of the disulfide bond on gold) was used.[32−34] For binary SAMs, the degree of phase segregation can be regulated by varying the fabrication parameters, such as the shaving speed.[25] The lateral heterogeneity ranged from near molecular level mixing to segregated nanodomains with different sizes and separations. The size and distribution of aldehyde domains in these nanostructures, therefore, can be regulated by varying the nanografting parameters to match the dimension of protein and the primary amine groups on individual protein surfaces for the investigation of covalent immobilization. Similar concepts may be applied to study protein adsorption *via* electrostatic van der Waals or hydrophobic interactions.

For the investigation of specific interactions, such as biorecognition, many arrays of nanostructures with designed feature sizes and separations must be produced. Nanografting is a serial process in nature presenting limitations such as vulnerability to thermal drift to maintain the designed geometry, subject to exchange due to prolonged soaking in thiol solution and the possibility of tip wear are the obstacles for

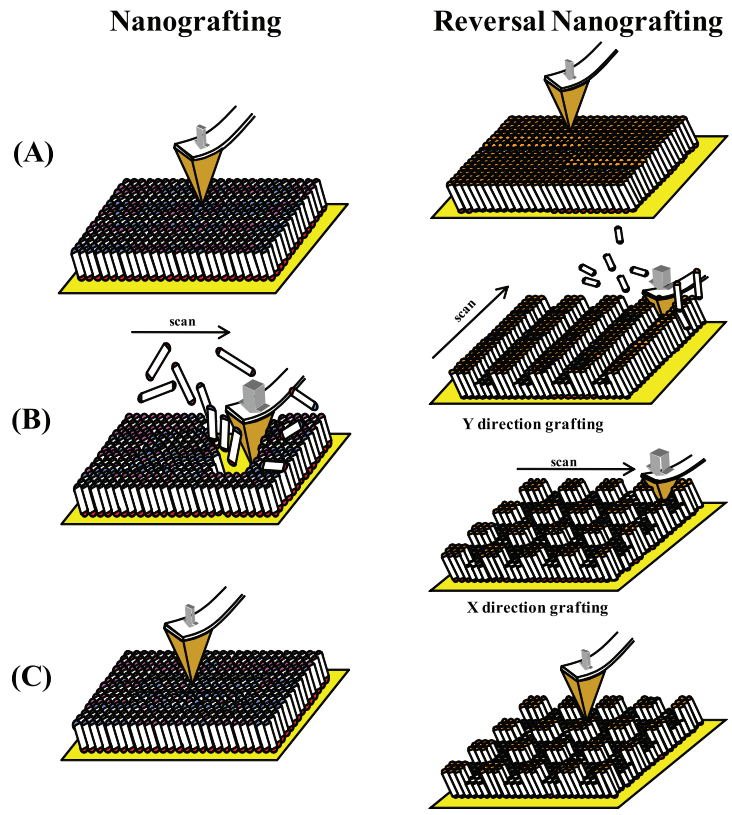

Figure 1. Nanografting and reversal nanografting process to reveal the key fabrication steps.

array production. Modifications to nanografting are made to overcome those limitations. The new and modified nanofabrication method, referred to as reversal nanografting, is illustrated in Figure 1. Similar to nanografting, this new method also has three main steps of imaging, shaving-and-replacement, and imaging again. In contrast to nanografting, the matrix SAM contains the protein binding termini, while the inert thiols are in the solution. During the shaving-and-replacement steps, these protein nonadherent thiols can be placed at a designed location to form boundaries between reactive thiols, and therefore, large sized protein binding structures can be divided into small sized nanostructures. By controlling the shaving size and the spacing between the shaving lines, arrays of nanostructures with desired size and numbers can be fabricated in a short period of time.

In terms of production of nanostructure arrays, reversal nanografting has the advantages of high fidelity to the design, excellent uniformity of the array elements, minimal subject to thermal drifts, and highly improved throughput. Reversal nanografting also allows for flexibility to select the inert component(s) to reach high self-assembly speed and to avoid or minimize the exchange reactions and/or to attain the designed local environment (*e.g.*, hydrophobic vs hydrophilic) surrounding the nanostructures.

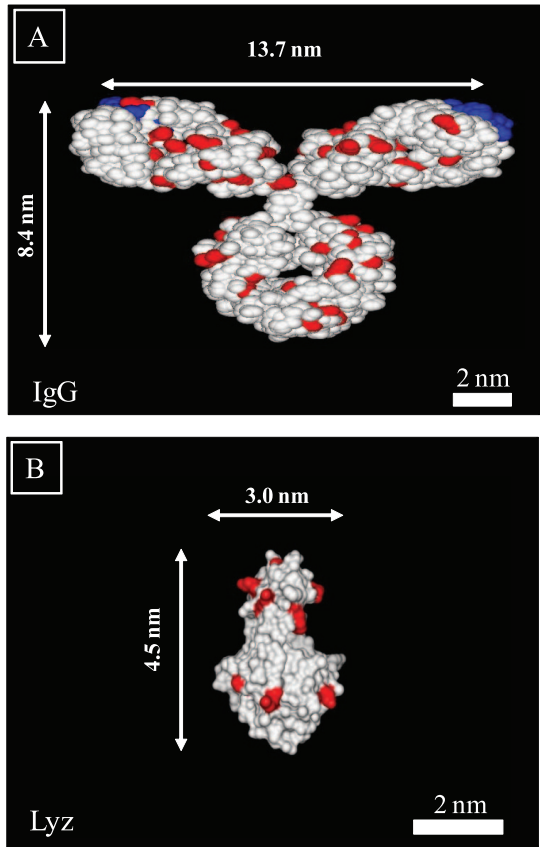

Figure 2. Structure of immunoglobulin G and lysozyme. (A) Y-Shaped immunoglobulin G molecule structure containing the 83 lysine groups (highlighted in red) and composed of two antigen binding fragments, Fab (highlighted in blue). (B) Lysozyme molecule with the 13 lysine groups highlighted in red. The molecular structures were rendered by Chimera from the Protein Data Bank.

Production of Three Arrays of Biotin Nanostructures Using Reversal Nanografting. The design of arrays of biotin nanostructures took the protein structure and antibody recognition reaction into consideration. The structure of an IgG was obtained from the protein data bank (ID code 1IGT) and is shown in Figure 2A to highlight the surface binding sites. Molecular graphics images were produced using the University of California, San Francisco (UCSF) Chimera package from the Resource for Biocomputing, Visualization, and Informatics at the UCSF (supported by NIH P41 RR-01081).[35] The Y-shaped IgG is composed of two antigen-binding fragments, Fab (highlight in blue color in Figure 2A), and a crystallizable fragment. Both fragments are heavily decorated with lysine groups. Two important features are (a) the antigen binding sites (*i.e.*, the Fab domains), for specific binding of IgG to surfaces, and (b) all lysine residues (highlighted in red in Figure 2), for covalent immobilization onto CHO termini of SAMs. The typical dimensions of IgG are approximately 14.5 nm × 8.5 nm × 4.0 nm, with antigen binding sites separated by 13.7 nm.[36] There are approximately 83 lysine groups per IgG.

Figure 3A shows three arrays of biotin nanostructures fabricated using reversal nanografting. The three arrays represent three characteristic scenarios for the engineered biotin nanostructures: (i) nanostructures whose domain size is smaller than the goat antibiotin IgG and the separation between nearest neighbors is also smaller than the Fab separation; (ii) nanostructures whose domain size is smaller while the separation between nearest neighbors matches the separation of two Fab domains in IgG; and (iii) nanostructures whose domain size is larger than IgG and separations match the separation of two Fab domains. A biotin-terminated SAM was formed by 48 h immersion of a bare gold thin film in a *N*-biotinyl-*N*′-(11-mercaptoundecyl)-3,6-dioxaoctane-1,8-diamine solution. The inert spacer molecules, hexanethiol, were nanografted into the biotin SAM, using reversal nanografting. Three nanostructures referred to as 1, 2, and 3 cover the total areas of 450 nm × 500 nm, 470 nm × 500, and 410 nm × 1065 nm, respectively, as shown in Figure 3A. The zoom-in images, 300 nm × 300 nm area, of the three arrays are shown in panel D, E, and F, respectively, from which the dimension of the nanostructures can be quantified (see Table 1).

Array 1, shown in Figure 3D, contains a 33 × 33 biotin nanoarray, with square features of 5.2 nm × 5.2 nm. The separation of each element from edge-to-edge is 4.3 ± 0.6 nm. The center-to-center separation among each nearest element is 9.2 ± 0.6 nm. The dimension of individual nanosquares is too small for the Fab to form bivalent binding. Among collisions of IgG with the nearest neighboring biotin nanosquares, most would not result in bivalent binding because the separation is too small, except in the extreme case where Fab collides with two far edges of the neighboring nanosquares. The probability of matched collisions is very slim, thus the coverage of IgG on array 1 is likely to be very low.

Array 2, as shown is Figure 3E, has 16 × 18 biotin-terminated nanostructures, with a feature size of 12.7 nm × 12.7 nm. The edge-to-edge separation distance is 5.9 ± 0.7 nm, and center-to-center separation is increased to 18.0 ± 1.2 nm. Array 2 provides excellent geometry matching to the Fab domains of the IgG (*i.e.*, 13.7 nm). Any collisions of Fab with the nearest neighbor nanosquares would satisfy the geometry required for bivalent recognition. The biorecognition occurs by bridging to the nanosquares. The third array has 8 × 18 elements, with rectangular features of 10.3 nm × 31.9 nm. Along the *x*-axis (long axis of each nanofeature), the separation distance between the neighboring biotin nanofeatures is 8.2 ± 1.9 and 40.2 ± 1.9 nm from edge-to-edge and center-to-center, respectively. Similarly, for the *y*-axis (short axis of each nanofeature), the separation distance between the neighboring biotin structures from edge-to-edge is 5.5 ± 0.7 nm. The center-to-center separation distance is 16.3 ± 0.7 nm. The geometry of array 3 allows biorecognition to occur within each feature or by bridging nearest neighbor nanostructures of biotin along various azimuthal direc-

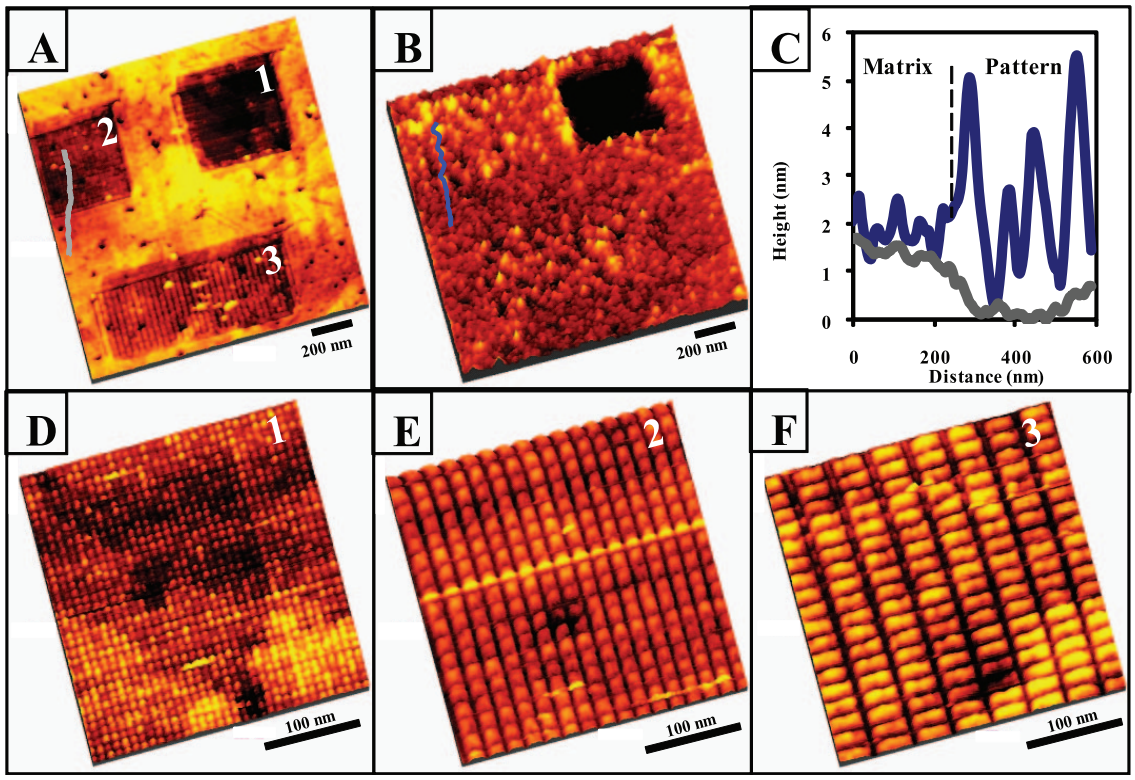

Figure 3. Antibiotin IgG reacts with thiolated biotin nanostructure arrays fabricated using reversal nanografting. (A) A 1500 nm × 1500 nm area revealing three different areas of nanoarrays of biotin produced using reversal nanografting as indicated by 1, 2, and 3. (B) The same area as (A) after antibiotin IgG injection. (C) A combined cursor plot as defined by the line in (A) and (B) is shown in order to reveal the local height change before and after exposure to the IgG solution. (D) A 300 nm × 300 nm zoom-in AFM topographic image of area 1. There are 1089 biotin nanofeatures with feature size of 5.2 nm × 5.2 nm. (E) A 300 nm × 300 nm zoom-in AFM topographic image of area 2. There are 288 nanofeatures with dimension of 12.7 nm × 12.7 nm. (F) A 300 nm × 300 nm zoom-in AFM topographic image of area 3. There are 144 nanofeatures with dimension of 10.3 nm × 31.9 nm.

tions. The differences between engineered nanostructures and the nanodomains in matrix SAMs are significant both qualitatively, square and rectangle domains *versus* ellipses, as well as quantitatively as summarized in Table 1.

Antibody Recognition of Biotin in the Presentation of SAMs and Nanostructures. The antigen (*i.e.*, biotin termini) present in three arrays of nanostructures and the surrounding SAM were exposed to the same goat antibiotin IgG solution, 10 μg/mL in 1× PBS buffer (pH 7.0), and were allowed to incubate for 30 min. Upon washing with 1% Tween 20, the surface was then imaged in PBS and is shown in Figure 3B. The presentation of biotin clearly impacted the subsequent protein adsorption, comparing Figure 3A with 3B. First, the coverage of IgG varies depending on the local environment of antigens. Only minute amounts of IgG, 15 ± 2 molecules, were seen in array 1, from Figure 3B, while more antibodies are found on nanostructures 2 and 3, 137 ± 5 and 155 ± 20, respectively. In the biotin SAM region in Figure 3B, the number of adsorbed protein is 607 ± 40. The number of proteins was counted using the follow-

TABLE 1. Antibody Recognition of Surface-Bound Biotin under Four Different Presentations

biotin SAMs	biotin nanostructure preparation	total area (nm × nm)	total number of features	feature size (nm × nm)	separation (nm)		matching to Fab sites	protein coverage (protein/μm²)
					edge-to-edge	center-to-center		
matrix	natural growth	entire Surface	nanodomains covering entire surface	13.2 × 7.0 (domain size)	4.8	10.9	excellent	450 ± 29
array "1"	reversal nanografting	450 × 500	3969	5.2 × 5.2	4.3	9.2	poor	67 ± 9
array "2"	reversal nanografting	470 × 500	961	12.7 × 12.7	5.9	18.0	excellent among nearest neighbor biotin nanosquares	582 ± 22
array "3"	reversal nanografting	410 × 1065	465	10.3 × 31.9	8.2	40.2	excellent within each and among nearest neighbor biotin nanostructures	355 ± 45
					5.5	16.3		

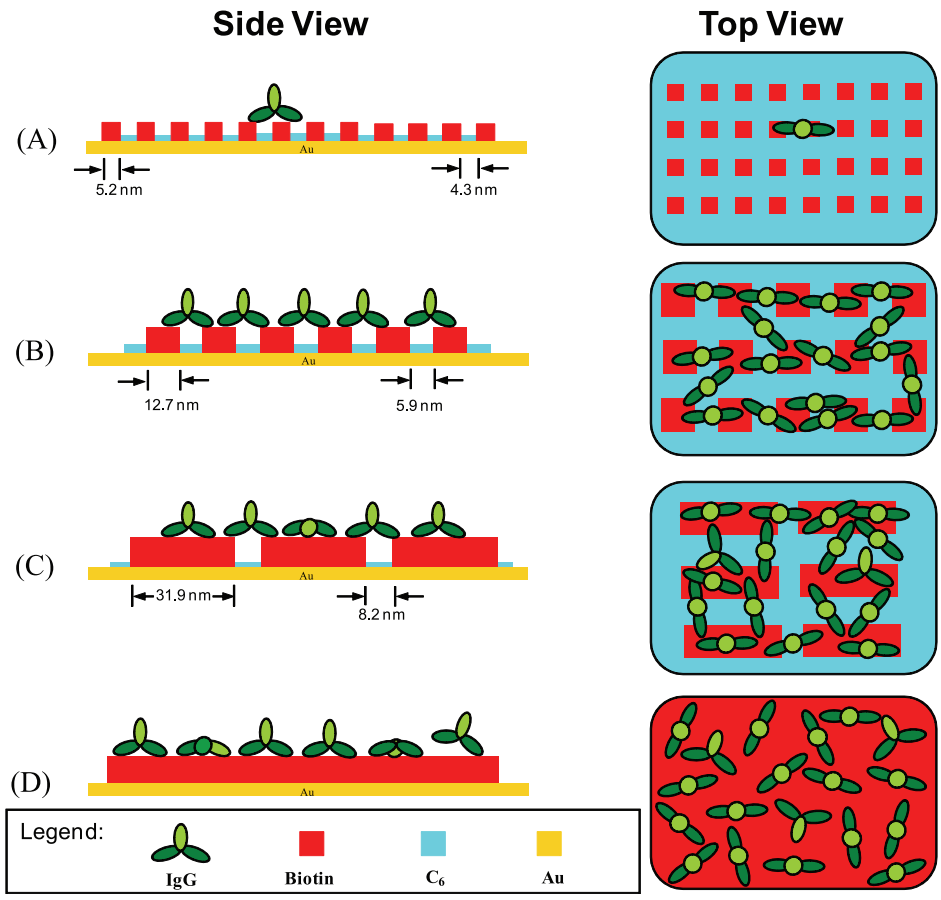

Figure 4. Antibiotin IgG (top view and side view) reacted with biotin nanofeatures at different scenarios: (A) feature size and separation of biotin, poorly match the goat-antibiotin IgG Fab domain; (B) feature size is too small while the separation between nearest neighbor nanostructure is excellent in matching the geometric separation of two Fab domains of IgG; and (C) the individual biotin nanofeatures provide an excellent match to the Fab domain, and excellent matching of the Fab domain to biotin also achieved among nearest neighbor biotin nanostructures. (D) IgG reacts among the nearest neighbor biotin domain.

ing dimensions as the threshold: 20 nm lateral widths and 5.8 nm in AFM apparent height, based upon individual IgG molecules imaged under AFM. This threshold is determined from protein molecules in the low coverage region and is consistent with previous AFM investigations.[12] For comparison, the protein coverage was quantified using the number of IgG molecules per μm^2: 67 $\pm$ 9, 582 $\pm$ 22, 355 $\pm$ 45, and 450 $\pm$ 29 IgG molecules per μm^2 for arrays 1, 2, 3, and matrix region, respectively. The morphology of the IgG molecules in array 2 differs from the rest by exhibiting brighter contrast, as shown in Figure 3B. The local height before and after exposure to the protein solution is shown in Figure 3C, where a combined cursor profile reveals clearly that IgG molecules on nanostructure 2 appear taller than that in the matrix region. This observation is consistent with the explanation that protein molecules on array 2 have a higher coverage and share similar lateral orientations in comparison to other regions. The higher degree of coverage and homogeneity manifests into less deformation under the AFM tip during contact imaging.

The observations above indicate that antibody recognition can be regulated by varying the geometry, allowing the availability in size and distance matching of surface-bound antigens, using reversal nanografting. This conclusion, based on the correlation between the structure of SAMs and three arrays of biotin nanostructures and the protein attachment, is illustrated schematically in Figure 4. Using the biotin SAM matrix as a reference, where biotin molecules are readily available for goat antibiotin IgG to attach, randomly orientated IgG were observed, as illustrated in Figure 4D. Nanoengineered areas reveal different outcomes. Figure 4A represents nanostructures such as array 1, whose elemental size is too small to accommodate one antibody binding. Since the distance between neighboring features (9.2 nm) does not match the geometric separation of two Fab binding domains (13.7 nm), the probability for goat antibiotin IgG bivalently binding to neighboring elements is also poor. As a result, little protein attachment is observed for nanostructures in array 1.

Figure 4B represents nanostructures (*e.g.*, array 2 in Figure 3A) whose feature size is too small for divalent antibody binding. However, the geometry among nearest neighbor nanofeatures matches the Fab binding to allow antibody recognition. Such geometry matching resulted in effective antibody recognition, as shown in Figure 3B and illustrated in Figure 4B. Even though array 2 was not designed to align the proteins, the immobilized protein layer exhibits a higher degree of homogeneous orientation in comparison to the randomly placed IgG onto the biotin SAM in the surrounding matrix. To demonstrate the robustness of this regulation, array 3 was designed to allow IgG to attach within each nanofeature and to bridge neighboring nanostructures along various azimuthal directions. In other words, array 3 is similar to the matrix SAM. As a result, the antibody recognition occurred in a similar fashion as on biotin SAMs, as revealed in Figure 3B and illustrated in Figure 4C.

The concept of regulations *via* nanolithography may be extended to the forward phase protein microarrays, where the specific orientation of the IgG molecules can be obtained by using Fc binding functional-

ities, such as protein A or G. Protein A or G can be immobilized on CHO-terminated SAM nanostructures. This attachment enables Fab fragments to face the solution for binding specific antigens. In dealing with a crude mixture protein, this methodology would also be useful by production of multiple arrays, each with functionality specific to targeted proteins, such as RGD-terminated nanostructures for integrin, and IgG nanostructures specific to F-actin, *etc*. This is analogous to the concept of multiplexing, except that nanografting enables nanoscale control. *In situ* characterization with resolution of individual proteins is also a benefit to verify adsorption and to determine protein coverage and orientation *in situ*.

Covalent Immobilization of IgG on Aldehyde Domains Presented in Naturally Grown and Nanografted Binary SAMs. Previously, we have demonstrated that nanografting can be utilized to regulate the lateral heterogeneity of binary SAMs, using a mixture of 1-hexanethiol and 1-octadecanethiol.[25] In this investigation, we extended the regulatory capability to binary SAMs with protein adhesive groups, such as aldehydes. Figure 5A is a 500 nm × 500 nm AFM topographic image revealing two nanografted rectangular patterns, at 180 nm × 120 nm and 220 nm × 205 nm, labeled as pattern 4 and 5, within the mixed SAM of C_6 and C_{10}CHO. The matrix SAM clearly exhibits phase segregation, as expected for SAMs formed from co-adsorption of C_6 and C_{10}CHO in solution.[25] The degree of heterogeneity in the two nanostructures (4 and 5) is less than the matrix by comparison, as shown in Figure 5A. Quantitative comparison may be extracted from zoom-in scans (100 nm × 100 nm) as shown in Figure 5B,C for the matrix and nanostructures, respectively. Each C_{10}CHO domain in the matrix region adopts irregular and elongated shapes with a typical domain size ranging from 8.4 to 19.7 nm on the long axis and from 4.7 to 10.8 nm on the short axis. The C_{10}CHO domain size in nanostructure 4 is less irregular, with 7.1 nm × 5.5 nm in dimension, and the distance between the neighboring C_{10}CHO domains from center-to-center and edge-to-edge is 12.1 and 6.5 nm, respectively. The quantitative information of the domain structures is summarized in Table 2.

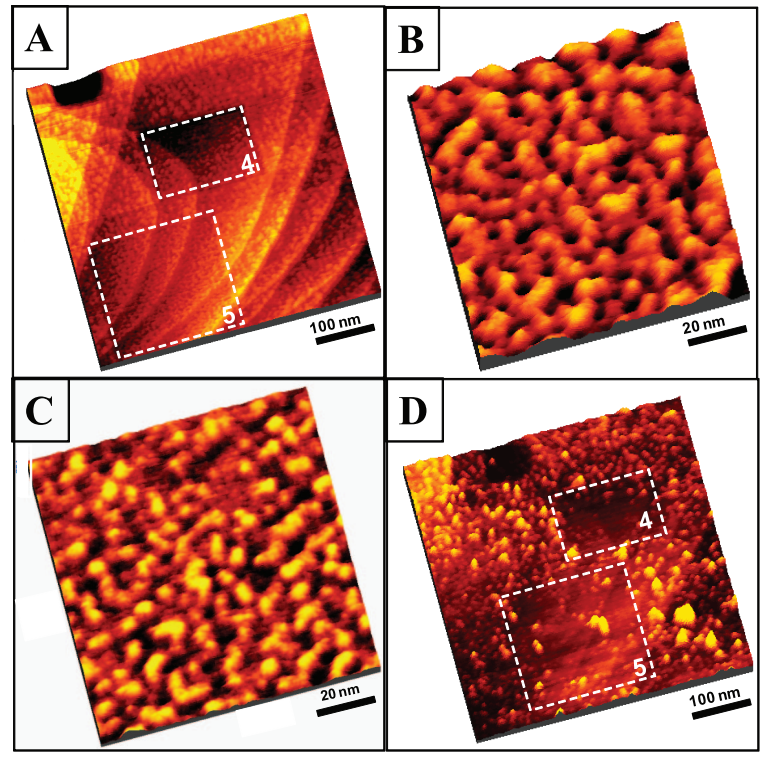

Figure 5. Binary mixed SAMs of hexanethiol and C_{10}CHO with a ratio of 1:1, total concentration 0.1 mM, formed from natural growth and nanografting. (A) AFM topographic image of the mixed SAM formed by co-adsorption of C_6 and C_{10}CHO from ethanol solution with mixed SAMs formed using the nanografting method. (B) High-resolution 100 nm × 100 nm image of the mixed SAM formed from natural growth. (C) A 100 nm × 100 nm nanostructure produced by nanografting from the mixed thiol solution, C_{10}CHO/C_6 (0.1 mM 1:1, using fabrication rate at 100 nm/s). (D) AFM topographic image of the same area after injection of 10 μg/mL rabbit IgG in 10 mM HEPES buffer (pH 6.8) for 30 min. AFM topographic image of the same area, after the surface was thoroughly washed with 1% Tween 20 to remove noncovalently bound proteins.

Upon incubation in a rabbit IgG solution, 10 μg/mL in 10 mM HEPES buffer (pH 6.8), for 30 min, the surface was washed with 1% Tween 20 and then imaged in HEPES medium. As shown in the 500 nm × 500 nm topographical image in Figure 5D, the protein adsorption varies based on the local structure of aldehyde domains. The lateral width of 20 nm and 1.5 nm in AFM apparent height was used as the threshold and guide for the immobilized IgG. There are approximately 580 ± 53, 27 ± 3, and 25 ± 4 IgG molecules in the matrix area and nanostructures 4 and 5, respectively. After normalization, the surface coverage of IgG on the surface of the naturally grown region is 2213 ± 212 proteins/μm^2, which is almost two times the coverage on nanoengi-

TABLE 2. Lateral Heterogeneity of Binary Component SAMs Prepared by Natural Self-Assembly and Nanografting

			domain separation (nm)		protein coverage
mixed SAMs	SAM preparation	typical domain size (nm × nm)	center-to-center	edge-to-edge	(protein/μm^2)
C_{10}CHO/C_6 (Matrix)	natural growth	12.6 × 7.4	14.4	5.1	2,213 ± 212
array "4"	nanografting	7.1 × 5.5	12.1	6.5	1,184 ± 138
array "5"	nanografting	8.4 × 6.7	10.1	5.0	625 ± 89
C_{10}CHO/C_6 (Matrix)	natural growth	15.8 × 10.9	20.1	8.4	1,923 ± 150
array "6"	nanografting	9.3 × 4.6	8.6	3.9	1,883 ± 111

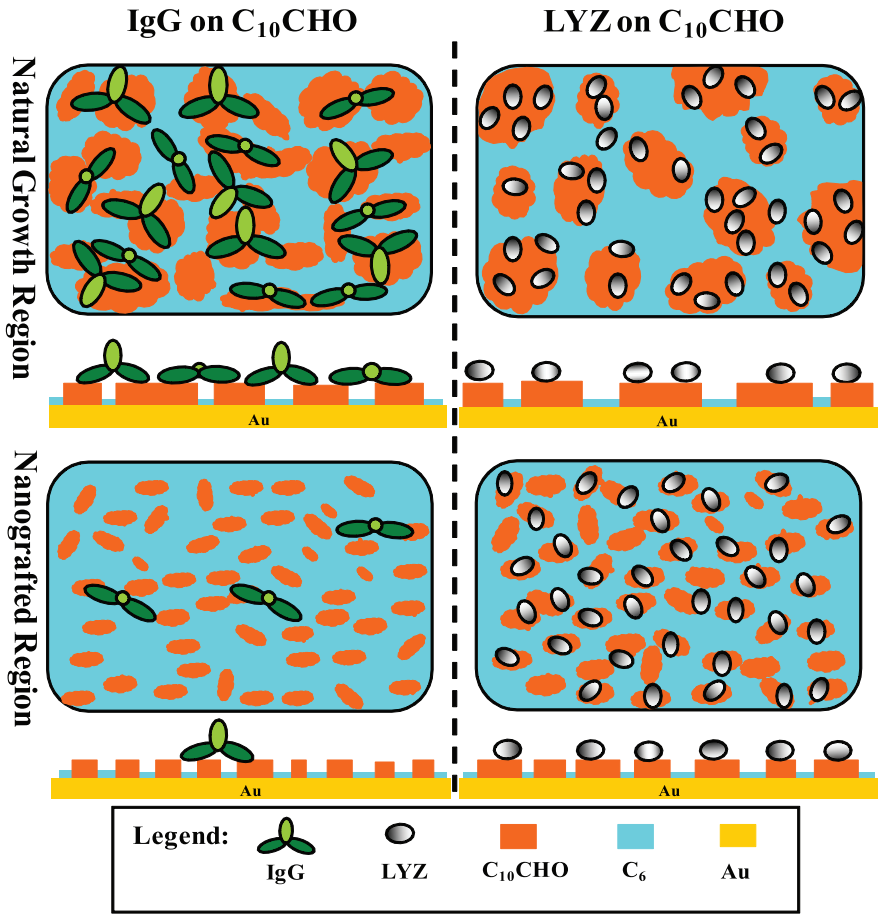

Figure 6. Schematic diagram of rabbit IgG and lysozyme immobilization on binary mixed SAMs of hexanethiol and C_{10}CHO at final ratio and concentration of 1:1, 0.1 and 0.02 mM, respectively, formed from natural growth and nanografting. The top view and side view of the immobilized IgG and lysozyme on the aldehyde-terminated nanostructure domain, both in natural growth and nanografted region, are presented.

neered structure 4 (1184 ± 138 protein/μm^2) and four times the coverage as nanostructure 5 (625 ± 89 protein/μm^2). This observation may be rationalized by the nature of protein immobilization onto aldehyde termini, that is, forming multiple covalent imine bonds with primary amine residues at the interface. All 83 lysine residues are highlighted as red to reveal their distributions within the IgG molecules (Figure 2). Assuming equal reactivity, the SAMs with CHO domains equal to or larger than the dimension of IgG (14.5 nm × 8.5 nm × 4.0 nm) would have higher probability to form multipoint bonds than small domains. In addition, the amine group at the Fab domain of IgG has a 50% higher reactivity than the Fc domain toward aldehyde groups according to the study by Hara *et al.*,[37] suggesting that the availability of CHO at 14.5 nm would facilitate the Fab bridging formation on surface aldehyde. Such availability can be provided by large (>14.5 nm) domains or by small domains with the desired separations. Taking both factors into consideration, the aldehyde domains in the matrix (shown in Figure 5B) exhibit a more optimized lateral size (10 nm) and separation (14.4 ± 1.2 nm) for IgG immobilization than that of the nanografted regions, where the domains are 30% smaller (7 nm) and the separation (12 nm) is not well matched to the amine residues in the Fab domain, as illustrated in Figure 6.

Covalent Immobilization of LYZ on Aldehyde Domains Presented in Naturally Grown and Nanografted Binary SAMs. To demonstrate the generic concept of regulating protein−surface interactions, a smaller protein, LYZ, was used. The SAM matrix is a mixture of C_6 and C_{10}CHO and was formed by soaking gold films into a 0.02 mM thiol solution with C_{10}CHO/C_6 = 1:1. Figure 7A is an AFM topograph of 500 nm × 500 nm with a 190 nm × 190 nm nanografted rectangular nanostructure 6 within. Zooming into both regions, the 100 nm × 100 nm scans shown in Figures 7B,C clearly reveal the difference of the phase segregation in the mixed SAM and the nanografted area. The bright contrast represents the C_{10}CHO domains, and the dark areas are the C_6 domains in the topographic images. Most of the C_{10}CHO domains in the matrix are 15.8 nm × 10.9 nm in size, with center-to-center and edge-to-edge separations around 20.1 and 8.4 nm, respectively. In the nanografted region shown in Figure 7, the aldehyde domains are smaller, 9.3 nm × 4.6 nm, with the center-to-center and edge-to-edge separations of 8.6 and 3.9 nm, respectively. Quantification of the domains is summarized in Table 2.

Figure 7D is the AFM topographic image showing the same area after exposing the surface to a LYZ solution of 5 μg/mL in 10 mM HEPES buffer (pH 6.8). Bright spots shown in Figure 7D correspond to LYZ attachment to SAM. The coverage in the matrix region at 1923 ± 150 LYZ/μm^2 is almost equal to that in the nanografted region, 1883 ± 111 LYZ/μm^2.

This observation may be rationalized by the size of LYZ and distribution of amine residues in the protein. As shown in Figure 2B, LYZ is ellipsoidal in shape and smaller than IgG, with dimensions of 4.5 nm × 3.0 nm × 3.0 nm. The 13 lysine groups are highlighted in red in Figure 2B to reveal the prospects for CHO attachment. Since the individual domains in the matrix and nanografted regions exceed the size of LYZ, similar coverage, assuming multipoint covalent bond formation between protein and CHO domains, is expected and is illustrated in Figure 6. For regulating LYZ attachment, smaller nanofeatures than the present work must be designed and produced. Therefore, the design and fabrication of SAM nanostructures

for covalent or electrostatic immobilization should take protein size and binding site distribution into consideration for effective immobilization regulation.

CONCLUSION

Using nanografting and reversal nanografting, we have demonstrated that nanostructures of protein binding termini can be produced with high spatial precision and with sufficient throughput for the investigation of subsequent protein attachment. The coverage as well as orientation of protein molecules can be regulated, to a large degree, by changing the dimension and separation of each nanoelement, in the case of biotin and antibiotin IgG reactions, and by changing the nanografting conditions, in the case of covalent immobilizations. The approach reported in this work is of generic importance because it provides alternative means to regulate protein immobilization on surfaces. The variation of protein coverage indicates the degree of control that this approach enables, which should be beneficial in the engineering of protein-based sensors where a wide dynamic range of analyte binding is necessary. In comparison to prior approaches, this new method has advantages of spatial precision and the ability to multiplex for micro- and nanodevice applications. Further, the strong dependence on the local structure and environment at the nanometer level further demonstrates the multivalent nature of protein attachment to surfaces. This multivalent interaction occurs between each protein molecule and surface ligands underneath, that is, in the length scale of several to tens of nanometers. Therefore, nanotechnology with molecular precision is the right tool for investigation and control of protein−surface interactions. Work is in progress to explore the regulation of more complex protein molecules and to further improve the accuracy and precision of this regulation.

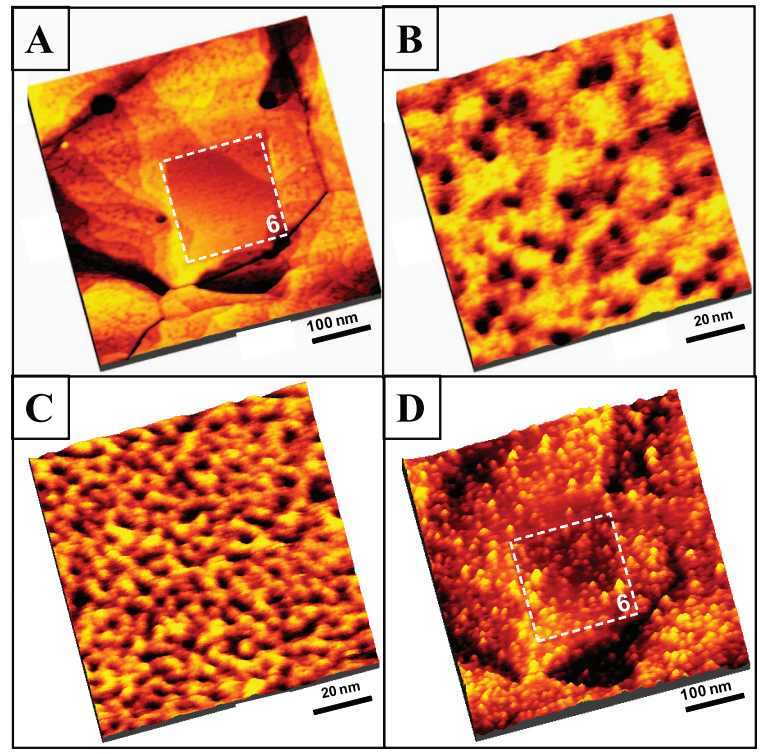

Figure 7. LYZ protein molecules covalently immobilized onto $C_{10}CHO$ domains within mixed $C_{10}CHO/C_6$ (0.02 mM, 1:1) SAMs formed from natural growth and nanografting processes. (A) 500 nm × 500 nm topographic image of the nanografted nanostructure surrounded by a mixed SAM from natural growth. (B) Zoom-in AFM image showing the phase separation of the mixed SAM in the surrounding area. (C) Zoom-in high-resolution image showing the detailed phase separation structures of the nanostructure. (D) AFM topographic image of the same area as in (A) after LYZ injection, 5 μg/mL lysozyme in HEPES buffer (pH 6.8) to the mixed SAMs for 10 min.

MATERIALS AND METHODS

Alkanethiol Materials. Hexanethiol (hereafter referred to as C_6), with a purity of more than 96%, was purchased from Sigma-Aldrich (Missouri, USA) and was used as received. Powder 11-mercapto-1-undecanal disulfide $[-S(CH_2)_{10}CHO]_2$ (referred to as $C_{10}CHO$ due to the cleavage of the disulfide bond on gold) was purchased from ProChimia (Gdansk, Poland).[32] Ethanol solvent of 99.99% purity was purchased from Gold Shield Chemical Co. (California, USA) and served as the solvent for all thiols.

Biotinylated Thiol, HSC_8-EG_3-biotin. Solvents used in the syntheses were purchased in capped DriSolv bottles and used directly without further purification and stored under argon. All glassware utilized in anhydrous conditions was flame-dried prior to use. Glass-backed TLC plates (Silica Gel 60 with a 254 nm fluorescent indicator) were used without further manipulation and stored over desiccant. Developed TLC plates were visualized under a short-wave UV lamp and stained with I_2 and/or by heating plates that were dipped in ammonium molybdate/cerium(IV) sulfate solution. Flash column chromatography (FCC) was performed using silica gel (32−63 μm) and employed a solvent polarity correlated with TLC mobility. NMR spectra (Varian INOVA 600 MHz, California, USA) were obtained using a 600 MHz instrument with $CDCl_3$ as a solvent, and chemical shifts were referenced to residual $CHCl_3$ (7.26 ppm) and $CDCl_3$ (77.1 ppm). High-resolution mass spectra were recorded at the UC Davis Molecular Structure Facility using MALDI-TOF (Applied Biosystems 4700 Proteomics Analyzer, California, USA) with internal calibration. Infrared spectra were acquired using an ATR-FTIR spectrometer (Spectrum 100 FTIR spectrometer, Massachusetts, USA).

***N*-Boc-*N*′-biotinyl-3,6-dioxaoctane-1,8-diamine (3).** To a solution of mono-Boc-protected amine **2** (2.04 g, 8.2 mmol) in 80 mL of DMF and 3.43 mL of TEA (25 mmol) stirred under argon was added D-biotin-2,3,5,6-tetrafluorobenzoate **1** (3.21 g, 8.8 mmol). The reaction mixture was stirred at room temperature for 24 h and then concentrated *in vacuo*. The resultant crude product was purified by FCC using a gradient of 16:1 to 8:1 CH_2Cl_2/MeOH to afford **3** as a white solid. NMR and mass spectral data of **3** are consistent with the literature.[38,39]

***N*-Biotinyl-3,6-dioxaoctane-1,8-diamine (4).** Reagent K[39] was prepared in a separate glass-stoppered flask and contained the following: 83% TFA, 5% phenol, 5% H_2O, 5% thioanisole, 3% 1,2-ethanedithiol. To **3** (1.26 g, 2.7 mmol) was added a 10 mL solution of Reagent K, and the mixture was stirred at room temperature for 1.5 h. The reaction mixture was then concentrated

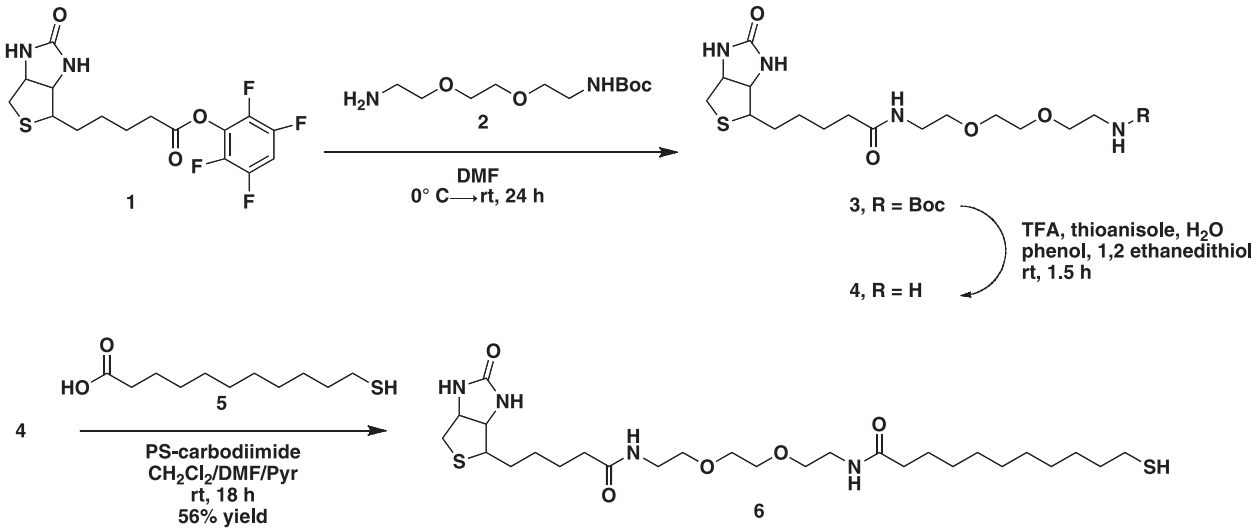

Scheme 1. Synthesis Route of *N*-Biotinyl-*N*′-(11-mercaptoundecyl)-3,6-dioxaoctane-1,8-diamine

and azeotroped several times with toluene. The crude product was purified by FCC using a gradient of 10:1 to 5:1 CH_2Cl_2/MeOH with 1% TEA added to afford **4** as brown oil. NMR and mass spectral data of **4** are consistent with the literature.[38,39]

***N*-Biotinyl-*N*′-(11-mercaptoundecyl)-3,6-dioxaoctane-1,8-diamine (6).** A solution of 11-mercaptoundecanoic acid **5** (260 mg, 1.2 mmol) in anhydrous CH_2Cl_2 (20 mL) was added to a suspension of PS-carbodiimide (1.42 g, 1.9 mmol) in 45 mL of anhydrous CH_2Cl_2 that was stirred for 5 min. After 5 min, a solution of **4** (353 mg, 0.94 mmol) in a 1:1 mixture of anhydrous DMF and pyridine (35 mL) was cannulated into the suspension. The reaction mixture was allowed to stir for 18 h at room temperature under argon. The resin was filtered off and washed with MeOH and CH_2Cl_2. The filtrate was concentrated, and the resulting material was purified by FCC using 10:1 CH_2Cl_2/MeOH to afford **3** (304 mg, 0.5 mmol) as a white solid in 56% yield (Scheme 1): ^{1}H NMR (600 MHz, $CDCl_3$) δ 6.49 (t, J = 5.7 Hz, 1H), 6.31 (t, J = 5.1 Hz, 1H), 6.26 (s, 1H), 5.25 (s, 1H), 4.52−4.50 (m, 1H), 4.33−4.31 (m, 1H), 3.62 (s, 4H), 3.57 (app t, J = 5.4 Hz, 4H), 3.50−3.39 (m, 4H), 3.17−3.14 (m, 1H), 2.92 (dd, J = 5.1, 12.9 Hz, 1H), 2.74 (d, J = 13.2 Hz, 1H), 2.52 (app q, J = 7.2 Hz, 2H), 2.23 (t, J = 7.5 Hz, 2H), 2.18 (t, J = 7.5 Hz, 2H), 1.75−1.57 (m, 12H), 1.23 (br s, 11H); ^{13}C NMR (150 MHz, $CDCl_3$) δ 173.6, 173.3, 163.8, 70.17, 70.14, 70.13, 70.0, 61.8, 60.2, 55.5, 40.6, 39.23, 39.20, 36.7, 36.0, 34.1, 29.55, 29.52, 29.47, 29.42, 29.1, 28.4, 28.16, 28.13, 25.8, 25.6, 24.7; MALDI-TOF-MS calcd for $C_{27}H_{50}N_4O_5S_2$ $[M + H]^+$ 575.32, found 575.35, $[M + Na]^+$ 597.32, found 597.33; FTIR 1552 (amide II band) 1643 (C═O amide, str), 1702 (C═O urea, str), 2852, 2922, 3287 (N−H str).[40,41]

Preparation of Self-Assembled Monolayers. The SAM preparation used in this study follows established procedures.[34,42] Gold (99,999%, Alfa Aesar, Massachusetts, USA) was deposited in a high-vacuum evaporator (Model DV502-A, Denton Vacuum, New Jersey, USA) at a base pressure below 2×10^{-7} Torr onto freshly cleaved mica substrates (clear ruby muscovite, S&J Trading Co., New York, USA). The mica was preheated and maintained at 350 °C before deposition using two quartz lamps mounted behind the mica. The substrate heating led to the formation of relatively large Au(111) terraces. Typical evaporation rates were 0.3 nm/s, and the thickness of the gold films ranged from 150 to 200 nm. After the evaporation, the gold thin films were annealed at 350 °C under vacuum for 30 min and allowed to cool to room temperature. The gold films were then transferred into the corresponding alkanethiol solutions within 5 min after removed from the vacuum chamber to avoid contamination. The two mixed $C_{10}CHO/C_6$ SAMs were formed in solutions containing an equal molar ratio and a total concentration of 0.1 and 0.02 mM, respectively. Biotin-terminated thiol SAMs were formed by immersing a gold film in a 0.1 mM solution for 48 h.

Preparation of Protein Solutions. LYZ (from hen egg, 95% purity), rabbit IgG (from rabbit serum, 95% purity), and goat antibiotin IgG (96% purity) were purchased from Sigma-Aldrich (Missouri, USA) and used as received. The protein solutions, such as rabbit IgG (10 μg/ml) and LYZ (5 μg/ml), were prepared in HEPES buffer (pH 6.8, 10 mM, Sigma-Aldrich, Missouri, USA). The goat antibiotin IgG was diluted to the desired concentration of 10 μg/mL using 1× PBS (pH 7.0, Sigma-Aldrich, Missouri, USA) before the immobilization process.

For the protein immobilization on surfaces, the concentrations of 10 μg/mL for IgG and 5 μg/mL for LYS were used to overwhelm the surface adhesion components in solution. Further, a CHO-terminated SAM was characterized in HEPES buffer (pH 6.8) without protein *in situ* as a control experiment. Little adsorption was observed in this blank test to confirm that the nature of the bright spots in the AFM topographs is due to protein attachment.

Atomic Force Microscopy Imaging and Analysis. The AFM utilized was a home-constructed, deflection-type scanning head that exhibits high mechanical stability. The scanner was controlled by an AFM 100 preamplifier and a STM 1000 electronics (RHK Technology, Inc. Michigan, USA). The AFM scanner was calibrated laterally *via* the periodicity of a mica(0001) surface (0.518 nm) and vertically using single atomic steps of a Au(111) (0.235 nm). Sharpened Si_3N_4 microlevers (Veeco Metrology Group, California, USA) with a force constant of 0.1 N/m were used for AFM imaging. Images were acquired using contact mode in specified liquid media. The typical imaging force is approximately 5 nN. Both domain size and domain spacing were measured quantitatively from more than 30 cursor profiles per image to get sufficient statistics. In mixed component SAMs, the $C_{10}CHO$ domain sizes were measured from the full width at half-maximum (fwhm) of the peaks, and the domain separations (center-to-center and edge-to-edge) were obtained from the separation distances between the peaks. In the array of biotin nanostructures, the feature size and edge-to-edge separation distances were measured from the fwhm.

For arrays 1, 2, 3, and 6, two additional experiments were completed in addition to the data reported here. For arrays 4 and 5, three more experiments were done to ensure reproducibility.

Acknowledgment. We thank Jessica Koehne and Susan G. Stagner at University of California, Davis, for helpful discussions. This work was supported by University of California, Davis; UC Discovery Grant in conjunction with Novartis; NIH (R21 GM077850-01) and NSF (CHE-0809977). Y.H.T. is a recipient of the Summer Graduate Student Researcher Award from University of California, Davis.

REFERENCES AND NOTES

1. Zhang, Y.; Sheng, S.; Shao, Z. Imaging Biological Structures with the Cryo Atomic Force Microscope. *Biophys. J.* **1996**, *71*, 2168–2176.
2. Zhou, D. J.; Wang, X.; Birch, L.; Rayment, T.; Abell, C. AFM Study on Protein Immobilization on Charged Surfaces at the Nanoscale: Toward the Fabrication of Three-Dimensional Protein Nanostructures. *Langmuir* **2003**, *19*, 10557–10562.
3. MacBeath, G.; Schreiber, S. L. Printing Proteins as Microarrays for High-Throughput Function Determination. *Science* **2000**, *289*, 1760–1763.
4. Ostuni, E.; Grzybowski, B. A.; Mrksich, M.; Roberts, C. S.; Whitesides, G. M. Adsorption of Proteins to Hydrophobic Sites on Mixed Self-Assembled Monolayers. *Langmuir* **2003**, *19*, 1861–1872.
5. Garno, J. C.; Amro, N. A.; Wadu-Mesthrige, K.; Liu, G. Y. Production of Periodic Arrays of Protein Nanostructures Using Particle Lithography. *Langmuir* **2002**, *18*, 8186–8192.
6. Wilson, D. L.; Martin, R.; Hong, S.; Cronin-Golomb, M.; Mirkin, C. A.; Kaplan, D. L. Surface Organization and Nanopatterning of Collagen by Dip-Pen Nanolithography. *Proc. Natl. Acad. Sci. U.S.A.* **2001**, *98*, 13660–13664.
7. Tan, J. L.; Tien, J.; Chen, C. S. Microcontact Printing of Proteins on Mixed Self-Assembled Monolayers. *Langmuir* **2002**, *18*, 519–523.
8. Abad, J. M.; Pita, M.; Fernández, V. M. Immobilization of Proteins on Gold Surfaces. In *Immobilization of Enzymes and Cells*; Guisan, J. M., Ed.; Humana Press: Berlin, Germany, 2006; pp 229−238.
9. Kwon, Y.; Han, Z.; Karatan, E.; Mrksich, M.; Kay, B. K. Antibody Arrays Prepared by Cutinase-Mediated Immobilization on Self-Assembled Monolayers. *Anal. Chem.* **2004**, *76*, 5713–5720.
10. Murphy, W. L.; Mercurius, K. O.; Koide, S.; Mrksich, M. Substrates for Cell Adhesion Prepared *via* Active Site-Directed Immobilization of a Protein Domain. *Langmuir* **2004**, *20*, 1026–1030.
11. Whitesides, G. M.; Ostuni, E.; Takayama, S.; Jiang, X.; Ingber, D. E. Soft Lithography In Biology and Biochemistry. *Annu. Rev. Biomed. Eng.* **2001**, *3*, 335–373.
12. Wadu-Mesthrige, K.; Amro, N. A.; Garno, J. C.; Xu, S.; Liu, G.-y. Fabrication of Nanometer-Sized Protein Patterns Using Atomic Force Microscopy and Selective Immobilization. *Biophys. J.* **2001**, *80*, 1891–1899.
13. Yang, T.; Baryshnikova, O. K.; Mao, H.; Holden, M. A.; Cremer, P. S. Investigations of Bivalent Antibody Binding on Fluid-Supported Phospholipid Membranes: The Effect of Hapten Density. *J. Am. Chem. Soc.* **2003**, *125*, 4779–4784.
14. Yang, T.; Jung, S. Y.; Mao, H.; Cremer, P. S. Fabrication of Phospholipid Bilayer-Coated Microchannels for On-Chip Immunoassays. *Anal. Chem.* **2001**, *73*, 165–169.
15. Mendes, P.; Yeung, C.; Preece, J. Bio-Nanopatterning of Surfaces. *Nanoscale Res. Lett.* **2007**, *2*, 373–384.
16. Holtz, B.; Wang, Y.; Zhu, X. Y.; Guo, A. Denaturing and Refolding of Protein Molecules on Surfaces. *Proteomics* **2007**, *7*, 1771–1774.
17. Krishnamurthy, V. M.; Kaufman, G. K.; Urbach, A. R.; Gitlin, I.; Gudiksen, K. L.; Weibel, D. B.; Whitesides, G. M. Carbonic Anhydrase as a Model for Biophysical and Physical−Organic Studies of Proteins and Protein−Ligand Binding. *Chem. Rev.* **2008**, *108*, 946–1051.
18. Oh, S. J.; Hong, B. J.; Choi, K. Y.; Park, J. W. Surface Modification for DNA and Protein Microarrays. *OMICS: J. Integr. Biol.* **2006**, *10*, 327–343.
19. Barbulovic-Nad, I.; Lucente, M.; Sun, Y.; Zhang, M.; Wheeler, A. R.; Bussmann, M. Bio-Microarray Fabrication Technique. *Crit. Rev. Biotechnol.* **2006**, *26*, 237–259.
20. Huang, Y. W.; Gupta, V. K. A SPR and AFM Study of the Effect of Surface Heterogeneity on Adsorption of Proteins. *J. Chem. Phys.* **2004**, *121*, 2264–2271.
21. Jung, H.; Yang, T.; Lasagna, M. D.; Shi, J.; Reinhart, G. D.; Cremer, P. S. Impact of Hapten Presentation on Antibody Binding at Lipid Membrane Interfaces. *Biophys. J.* **2008**, *94*, 3094–3103.
22. Johnson, R. D.; Wang, Z. G.; Arnold, F. H. Surface Site Heterogeneity and Lateral Interactions in Multipoint Protein Adsorption. *J. Phys. Chem.* **1996**, *100*, 5134–5139.
23. Gestwicki, J. E.; Cairo, C. W.; Mann, D. A.; Owen, R. M.; Kiessling, L. L. Selective Immobilization of Multivalent Ligands for Surface Plasmon Resonance and Fluorescence Microscopy. *Anal. Biochem.* **2002**, *305*, 149–155.
24. Mammen, M.; Choi, S. K.; Whitesides, G. M. Polyvalent Interactions in Biological Systems: Implications for Design and Use of Multivalent Ligands and Inhibitors. *Angew. Chem., Int. Ed.* **1998**, *37*, 2754–2794.
25. Yu, J. j.; Tan, Y. H.; Li, X.; Kuo, P. K.; Liu, G. y. A Nanoengineering Approach to Regulate the Lateral Heterogeneity of Self-Assembled Monolayers. *J. Am. Chem. Soc.* **2006**, *128*, 11574–11581.
26. Xu, S.; Liu, G. Y. Nanometer-Scale Fabrication by Simultaneous Nanoshaving and Molecular Self-Assembly. *Langmuir* **1997**, *13*, 127–129.
27. Xu, S.; Miller, S.; Laibinis, P. E.; Liu, G. Y. Fabrication of Nanometer Scale Patterns within Self-Assembled Monolayers by Nanografting. *Langmuir* **1999**, *15*, 7244–7251.
28. Lee, K.-B.; Park, S.-J.; Mirkin, C. A.; Smith, J. C.; Mrksich, M. Protein Nanoarrays Generated By Dip-Pen Nanolithography. *Science* **2002**, *295*, 1702–1705.
29. Woodson, M.; Liu, J. Functional Nanostructures from Surface Chemistry Patterning. *Phys. Chem. Chem. Phys.* **2007**, *9*, 207–225.
30. Liu, M.; Amro, N. A.; Chow, C. S.; Liu, G. y. Production of Nanostructures of DNA on Surfaces. *Nano Lett.* **2002**, *2*, 863–867.
31. Liu, M.; Amro, N. A.; Liu, G.-y. Nanografting for Surface Physical Chemistry. *Annu. Rev. Phys. Chem.* **2008**, *59*, 367–386.
32. Ishida, T.; Yamamoto, S.; Mizutani, W.; Motomatsu, M.; Tokumoto, H.; Hokari, H.; Azehara, H.; Fujihira, M. Evidence for Cleavage of Disulfides in the Self-Assembled Monolayer on Au(111). *Langmuir* **1997**, *13*, 3261–3265.
33. Nuzzo, R. G.; Fusco, F. A.; Allara, D. L. Spontaneously Organized Molecular Assemblies. 3. Preparation and Properties of Solution Adsorbed Monolayers of Organic Disulfides on Gold Surfaces. *J. Am. Chem. Soc.* **1987**, *109*, 2358–2368.
34. Nuzzo, R. G.; Zegarski, B. R.; Dubois, L. H. Fundamental Studies of the Chemisorption of Organosulfur Compounds on Gold(111). Implications for Molecular Self-Assembly on Gold Surfaces. *J. Am. Chem. Soc.* **1987**, *109*, 733–740.
35. Pettersen, E. F.; Goddard, T. D.; Huang, C.; Couch, G. S.; Greenblatt, D. M.; Meng, E. C.; Ferrin, T. E. UCSF Chimera—A Visualization System for Exploratory Research and Analysis. *J. Comput. Chem.* **2004**, *25*, 1605–1612.
36. Bagci, H.; Kohen, F.; Kuscuoglu, U.; Bayer, E. A.; Wilchek, M. Monoclonal Anti-Biotin Antibodies Simulate Avidin in the Recognition of Biotin. *FEBS Lett.* **1993**, *322*, 47–50.
37. Endo, N.; Umemoto, N.; Kato, Y.; Takeda, Y.; Hara, T. A Novel Covalent Modification of Antibodies at their Amino Groups with Retention of Antigen-Binding Activity. *J. Immunol. Methods* **1987**, *104*, 253–258.
38. Sigal, G. B.; Mammen, M.; Dahmann, G.; Whitesides, G. M. Polyacrylamides Bearing Pendant Alpha-Sialoside Groups Strongly Inhibit Agglutination of Erythrocytes by Influenza Virus: The Strong Inhibition Reflects Enhanced Binding through Cooperative Polyvalent Interactions. *J. Am. Chem. Soc.* **1996**, *118*, 3789–3800.
39. King, D. S.; Fields, C. G.; Fields, G. B. A Cleavage Method Which Minimizes Side Reactions Following FMOC Solid-Phase Peptide-Synthesis. *Int. J. Pept. Protein Res.* **1990**, *36*, 255–266.

40. Nolting, B.; Yu, J. J.; Liu, G.-y.; Cho, S. J.; Kauzlarich, S.; Gervay-Hague, J. Synthesis of Gold Glyconanoparticles and Biological Evaluation of Recombinant Gp120 Interactions. *Langmuir* **2003**, *19*, 6465–6473.
41. Yu, J.-J.; Nolting, B.; Tan, Y. H.; Li, X.; Gervay-Hague, J.; Liu, G.-y. Polyvalent Interactions of HIV-gp120 Protein and Nanostructures of Carbohydrate Ligands. *Nanobiotechnol.* **2005**, *1*, 201–210.
42. Amro, N. A.; Xu, S.; Liu, G. y. Patterning Surfaces Using Tip-Directed Displacement and Self-Assembly. *Langmuir* **2000**, *16*, 3006–3009.